



Contour integration in color vision: a common process for the blue–yellow, red–green and luminance mechanisms?

Kathy T. Mullen *, William H. A. Beaudot, William H. McIlhagga

McGill Vision Research, Department of Ophthalmology, McGill University, 687 Pine Avenue West (H4-14), Montreal, Canada H3A 1A1

Received 18 July 1998; received in revised form 18 November 1998

Abstract

We compare the performance of the red–green, blue–yellow and luminance postreceptoral mechanisms on a contour integration task requiring the linking of oriented Gabor elements across space to extract a winding ‘path’ or contour. We first establish that for all three mechanisms curvature and contrast are independent; losses in performance due to one cannot be compensated by changes in the other. We then compare contour integration by the three mechanisms using a method that controls for their differences in cone contrast thresholds. Our results show that despite the poor orientation discrimination thresholds and poor spatial sampling found for the blue–yellow mechanism, all three mechanisms perform similarly on contour integration over a wide range of curvatures. Furthermore, all three mechanisms have the same dependence on path curvature. We also investigate the effects of adding external orientation noise. Our results imply that the internal orientation noise for extracting ‘aligned’ path elements is similar in the three mechanisms and for all path curvatures, and the relative efficiencies are also similar for the three mechanisms. To account for our results, we propose that the three postreceptoral mechanisms use a common contour integration process. This linking process, however, cannot be color-blind; our last experiment shows that linking between different chromatic mechanisms or between opposite spatial phases disrupts contour integration. We thus propose that the common integration process remains sensitive to the color contrast and phase of its inputs. © 2000 Elsevier Science Ltd. All rights reserved.

Keywords: Color vision; Isoluminance; Red–green and blue–yellow mechanisms; Contour integration

1. Introduction

The role of color in form perception has a controversial history. The results of the early experiments on isoluminance suggested that color vision had a minimal input to a range of spatial tasks, such as shape from shading, illusory contours, monocular perspective and cyclopean form perception (Lu & Fender, 1972; Gregory, 1977; Livingstone & Hubel, 1987, 1988; Gregory & Heard, 1989), leading to the suggestion that color plays only a subordinate role in the extraction of form. According to this initial view of color vision, termed the ‘coloring book’ model, it is the luminance contours and edges of the image that are primarily extracted and used to divide the image up into a number of non-overlapping areas (McIlhagga & Mullen, 1997). The color

of these areas may be used in the linking process, since areas of a similar color are likely to be parts of a common object, but color has no direct input to the main process of contour or form extraction. Thus under this scheme, color vision need only have lowpass spatial filters and, if truly subordinate, should be incapable of seeing form by itself.

Another possible model, following Barrow and Tenenbaum’s (1978) idea of ‘intrinsic images’, attributes a more active role to color vision (Mullen & Kingdom, 1990; McIlhagga & Mullen, 1997). It proposes that both the color and the luminance system are capable of extracting edges from the visual scene and so dividing the image into distinct regions. Since color and luminance edges are not always coincident, as in the case of shadows, the color and luminance systems are performing essentially the same computations, but different images are created. Color edges that coincide with the luminance edges indicate object boundaries, and any remaining luminance edges indicate a change in the

* Corresponding author. Tel.: +1-514-842-1231, ext. 4757; fax: +1-514-843-1691.

E-mail address: kmullen@violet.vision.mcgill.ca (K.T. Mullen)

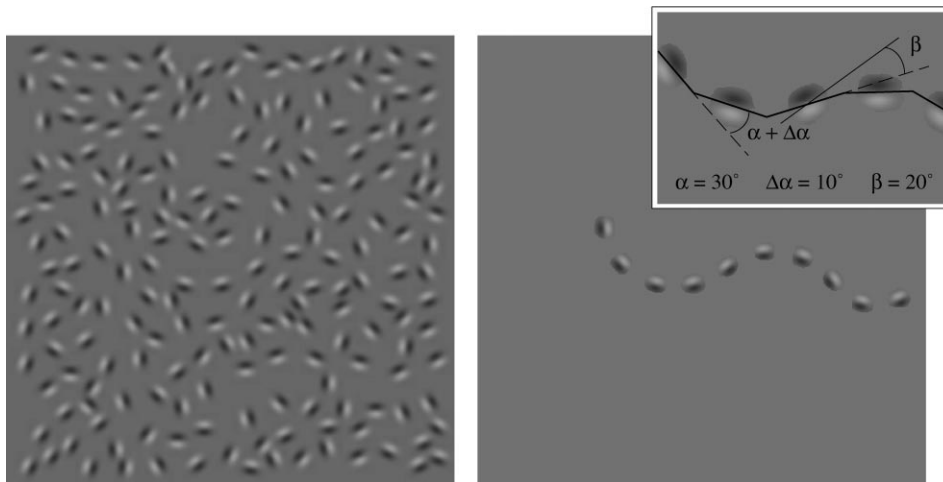


Fig. 1. Left panel: An example of the stimulus. The ‘path’ is difficult to detect. Experienced subjects perform at around 65–75% correct under our presentation conditions. Right panel: The path is shown separated from the background elements. It is a chain of ten Gabor elements which vary systematically in their orientation, as described in the inset. Inset: The path is made up of ten backbone line segments. The orientation difference between each successive line segment is given by the angle α which in this case is $\pm 30^\circ$. α determines the path curvature. $\Delta\alpha$ is a small orientation jitter added to α and is uniformly distributed between $\pm 10^\circ$. β gives the orientation of the Gabor element with respect to the backbone element. Unless otherwise stated β is 0.

illuminant intensity. The intrinsic images model implies firstly that color vision will have the necessary early processing capabilities for form perception, and secondly that color vision can independently extract object boundaries in the absence of a contribution from luminance contrast. Evidence suggests that color vision has bandpass spatial filters within its overall lowpass contrast sensitivity envelope (Switkes, Bradley & De Valois, 1988; Losada & Mullen, 1995), which also display orientation tuning (Bradley, Switkes & De Valois, 1988; Webster, De Valois & Switkes, 1990), and disparity selectivity (Simmons & Kingdom, 1994). Furthermore, it has been shown that red–green color contrast can be used as a basis for contour integration (McIlhagga & Mullen, 1996), for vernier alignment (Krauskopf & Farell, 1991), and that red–green isoluminant textures can be segregated (McIlhagga, Hine, Cole & Snyder, 1990). Thus while the idea that color vision is ‘form-blind’ gained early credence from some convincing demonstrations of the failures of color vision at isoluminance (Livingstone & Hubel, 1987; Gregory & Heard, 1989), the subsequent psychophysical investigations have suggested that color vision retains all the early visual processing capabilities for form perception.

In this paper, we investigate and compare the factors limiting the performances of the red–green, blue–yellow and luminance postreceptoral mechanisms on a contour integration task. If color vision is deficient in the early extraction of object boundaries we might expect it to be manifest on this task, which requires long range integrative or linking processes at a cortical level. The stimulus, shown in Fig. 1, was first used for the investigation of luminance vision by Field, Hayes and Hess (1993). A set

of ten oriented Gabor elements, placed along a winding contour or ‘path’, are embedded in a field of pseudo-randomly scattered and randomly oriented Gabor elements. The task is to detect the presence of the ‘path’, and indicates how successful the visual system is at linking the orientation of the elements. The more winding (curvy) the path becomes, the harder it is to detect. Crucially, path stimuli are well detected only if the Gabor elements are aligned along the path direction. Placing elements orthogonal to the path direction dramatically reduces performance, and randomly orienting them renders it invisible (Field et al., 1993). Psychophysical experiments such as these have shown that orientation is a key feature in this linking task. The importance of orientation in our experiments is in distinction to the grouping process that operate in the Ishihara plates or in the chromatic spatial alignment task of Kingdom, Moulden and Collyer (1992). In the Ishihara task, the grouping occurs on the basis of a common color and the dots have no intrinsic orientation. In our stimuli, the common orientation of the elements defines the path, and all elements of the stimulus usually have the same coloration.

A second important feature of the task is that it is long range, requiring the consecutive linking of the elements along a path length of up to 13° in our stimulus. It has been argued that, in the fovea and parafovea, achromatic path detection cannot be supported by a simple linear filtering model which describes path detection by a single, spatially tuned unit with a large receptive field (Hess & Dakin, 1997)¹.

¹ In the periphery, 10° and over, the task can be explained by simple linear filtering (Hess & Dakin, 1997) so reducing its usefulness as a measure of contour integration.

Instead, path detection probably depends on integrative processes among cortical neurons that analyze different orientations in different regions of visual space. This two stage process, local edge detection followed by boundary integration, is used in a number of computational approaches to image segmentation (Marr, 1982; Grossberg & Mingolla, 1985; Parent & Zucker, 1989; Heitger & von der Heydt, 1993).

In this paper, we investigate some of the possible limitations of the performance of the red–green, blue–yellow and achromatic mechanisms on the contour integration task, and compare these limitations in the three mechanisms. It is worth noting that previous investigations of color and spatial structure have generally excluded the blue–yellow mechanism. Yet including this mechanism allows the early spatial sampling limitations on the contour integration task to be tested since, in comparison to the other two, the blue–yellow mechanism is supported by a very sparse distribution of S-cones (Williams, Collier & Thompson, 1983; Curcio, Allen, Sloan, Lerea, Hurley, Klock & Milam, 1991) and postreceptoral neurons (Dacey & Lee, 1994).

In the first group of experiments we investigate the joint roles of cone contrast and curvature in limiting path detection. In the second group, we investigate the role of visual field location on the contour integration task, since there are marked differences in the distributions of the three postreceptoral mechanisms away from the fovea. In the third group, we determine whether performance is limited by the encoding of the orientation of the individual stimulus elements in the three mechanisms. In the fourth group, we compare the effects of added external orientation noise on contour integration by the three postreceptoral mechanisms. In the last set of experiments, we determine whether contour elements can be linked between different postreceptoral mechanisms, and whether the cardinal directions have any special saliency for the linking process.

2. Methods

2.1. Stimuli

Stimuli consisted of a pseudo-random scattering of Gabor elements covering a square area with sides of 14° (see Fig. 1 for an example). The subject's task was to detect a 'path' which consisted of a set of ten oriented Gabor elements aligned along a single contour, embedded in the background of similar, randomly oriented Gabor elements. Inspection of Fig. 1 (left panel) reveals that the path in the example winds horizontally across the figure.

Gabor elements were odd symmetric and used to limit the spatial bandwidth of the stimuli. The peak spatial frequency of the elements was kept relatively low to reduce luminance artifacts arising from chromatic aberration (Bradley, Zang & Thibos, 1992). The Gabor elements are defined by:

$$g(x, y, \theta) = c \sin(2\pi f(x \sin \theta + y \cos \theta)) \exp - \left(\frac{x^2 + y^2}{2\sigma^2} \right) \quad (1)$$

where θ is the element orientation in degrees, (x, y) is the distance in degrees from the element center, and c is the contrast. The sinusoidal frequency (f) is 1.5 cpd, and the space constant (σ) is 0.17° .

The no-path stimulus was constructed as follows. The stimulus area was divided into a 14×14 grid of equally sized cells (each 1° square). A Gabor element of random orientation was placed in each cell so that each cell contained the center of only one Gabor element. This pseudo-random placement prevents clumping of the elements. Overlap of the elements was also prevented by restricting the placement of their centers within the cell. The average distance between neighboring Gabor elements was 1.3° . It was sometimes impossible to place a Gabor element in its cell because it was too close to elements previously placed. This produced an empty cell; no more than eight empty cells were permitted in a display, and the average number was four.

The path stimulus can be considered as two parts, the ten path elements themselves and the background elements, as illustrated in Fig. 1 (right panel) (see also McIlhagga & Mullen, 1996). The path has a 'backbone' of ten invisible line segments, of randomly selected lengths between 1.2 and 1.4° . The shape of the backbone is controlled by the curvature parameter α (path angle) which determines the angle difference between adjacent backbone elements. Higher values of α produce more curvature in the path. Primarily to avoid the occurrence of straight paths when $\alpha = 0^\circ$, an orientation jitter uniformly distributed between $\pm 10^\circ$ was added to the path curvature. Gabor elements were placed in the middle of each line segment. The orientation of the Gabor elements along the line segment of the backbone is termed β (Fig. 1, inset). In general, β is 0 and element orientation is the same as that of the line segment, but in some experiments β was varied to produce orientation noise in the path. Finally, to avoid random closure of the paths with a high curvature, which can affect detection (Elder & Zucker, 1993; Kovacs & Julesz, 1993), paths which looped back on themselves were discarded. The entire path was pasted into the display at a random location with the restrictions that the centers of the Gabor elements occupied different cells, and that at least one path element passed through the central 3° of the stimulus. The remaining

empty cells were filled with randomly oriented Gabor elements.

Control measurements ensured that no spurious cues could be used for path detection. In particular we ascertained that the presence of the path does not affect the local densities of the elements since the averaged distance between path elements and between background elements is the same and the number of empty neighboring cells are the same for both path and background elements. Furthermore, the number of empty cells is the same for both path and no-path stimuli indicating no global density changes. If neither density nor proximity are cues, path visibility should be due only to the alignment of the elements of the path since nothing else distinguishes path element from background element. This was confirmed in a control experiment in which the orientation of the path elements was randomized.

2.2. Chromatic representation of the stimuli

Stimuli were defined within a three-dimensional cone contrast space in which each axis represents the quantal catch of the L , M and S cone types normalized with respect to the white background. The spectral emissions of the red, green and blue guns of the monitor were calibrated at the National Research Council of Canada using a Photo Research PR-700-PC SpectraScan. The Smith and Pokorny fundamentals were used for the spectral absorption of the L , M and S cones. These data allowed a linear transform to be calculated specifying phosphor contrasts required for given cone contrasts (Cole & Hine, 1992).

Stimulus chromaticity and contrast is given by a vector direction and magnitude, respectively, within the cone contrast space. In most experiments only the three cardinal stimuli were used. These are designed to isolate each of the three different postreceptoral mechanisms. A cardinal direction for a given mechanism is the unique direction orthogonal to the vector directions of the other two mechanisms. Previous studies have estimated the red–green, blue–yellow and luminance mechanism directions to be approximately; $L - M$, $S - 0.5(L + M)$ and $3L + M$ (Cole, Hine & McIlhagga, 1993; Sankeralli & Mullen, 1996). From these the calculated luminance and blue–yellow cardinal directions are $L + M + S$ (the achromatic direction) and S , respectively. The wide inter-subject variability found for the luminance mechanism affects the specification of the red–green cardinal direction. Thus the red–green isoluminant direction was determined for each subject individually using a motion nulling technique (Anstis & Cavanagh, 1983) for a patch of grating (1.5 cpd, 3.6° square, foveal) presented in apparent motion, as previously described for this apparatus (McIlhagga & Mullen, 1996). Since the red–green isoluminant direction is

specified within the $L - M$ cone contrast plane, it is not orthogonal to the blue–yellow mechanism. Any resulting cross stimulation of the blue–yellow mechanism will be small, and given the very low cone contrast sensitivity of the blue–yellow mechanism relative to the red–green (Sankeralli & Mullen, 1996) is highly unlikely to influence the results.

2.3. Apparatus and protocol

Stimuli were displayed on a Sony Trinitron monitor with a Sun Sparcstation 2 computer. The monitor was driven by 8-bit D/A converters on a 24-bit framebuffer. The monitor was gamma corrected in software with lookup tables using luminance measurements obtained from a United Detector Technology Optometer (UDT S370) fitted with a 265 photometric sensor. The monitor was viewed at a distance of 60 cm in a blacked out room. The mean luminance of the display was 14.2 cd/m².

A 2AFC task was used to measure the subject's ability to detect the path. Each 2AFC stimulus pair consisted of a path and no-path stimulus, randomly selected, and the observer's task was to detect the stimulus containing the path. Stimuli were displayed for 0.5 s with abrupt onset and offset, each cued by a beep. Feedback was given. A fixation mark appeared briefly before the stimulus onset. Stimuli were generated online, and a new stimulus was generated for each presentation. For each block of trials the path curvature was fixed. Practice trials were typically run before the experiment commenced until the subject was familiar with the task. Normally several blocks of trials were performed consecutively. The number of trials per data point is given in the figure legends. The three observers were the authors, all with normal color vision.

3. Results

3.1. Contour integration within a cone contrast space

In this experiment we measure contour integration in 12 different directions in a three-dimensional cone contrast space. Thresholds for path detection were obtained with a 2AFC method of constant stimuli using four to five different cone contrast levels. Data were fitted with a Weibull function from which a path detection threshold was derived (at 82% correct). The path curvature was fixed at 15° for KTM and 20° for WHM. In Fig. 2, results are shown for the $L - M$ plane (top panels) and for the S , $L + M$ plane (bottom panels). In each panel, the cardinal directions are marked as RG, BY and Ach. The results show that although the contrast required for detection varies with the vector direction, there is no direction in which path detection fails.

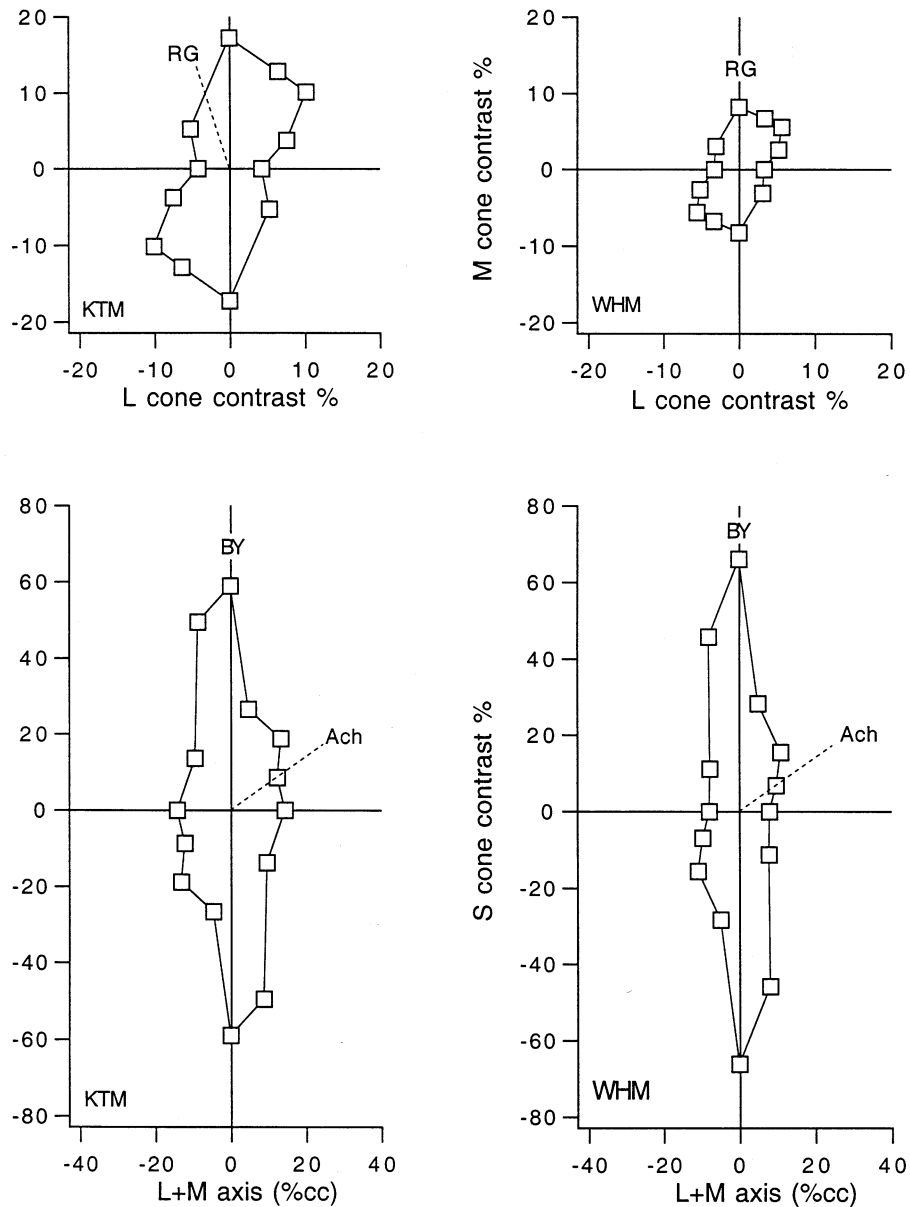


Fig. 2. Top panels: Path detection thresholds plotted within an L , M cone contrast space. RG indicates the direction of the cardinal axis for the red–green mechanism (the red–green isoluminant direction, as determined for each subject). Note that WHM’s isoluminant direction is superimposed on to the M cone axis; this is because of the very high $L:M$ cone ratio of his luminance mechanism. Lower panels: Path detection thresholds plotted within the S , $L+M$ plane. BY and Ach indicate the blue–yellow and achromatic cardinal directions respectively. Note the blue–yellow cardinal direction corresponds to the S -cone axis. Path curvature was 15° for KTM and 20° for WHM. Thresholds were determined using a method of constant stimuli with four to five contrasts per psychometric function presented 40 times each.

For the L – M plane (upper panels) the path detection threshold contour is not especially elongated, whereas path detection thresholds in the S versus $L+M$ plane (lower panels) show a considerable elongation along the S cone axis.

In general, previous results have shown that detection threshold contours in the L – M plane for foveal Gabor stimuli have a high elongation in the first (+ L , + M) and third (– L , – M), quadrants reflecting the much greater sensitivity of the foveal red–green mechanism compared to the luminance mechanism (e.g.

Cole et al., 1993; Sankeralli & Mullen, 1996). The absence of this elongation in our path detection results is most probably due to the distributed nature of our stimuli. The high contrast sensitivity of the red–green relative to the luminance mechanism disappears rapidly at parafoveal locations (Mullen, 1991; Mullen & Kingdom, 1996).

Our impression was that at path detection threshold (when the presence of the contour is just detectable), the individual Gabor elements were all clearly visible. To confirm this, we measured detection thresholds for

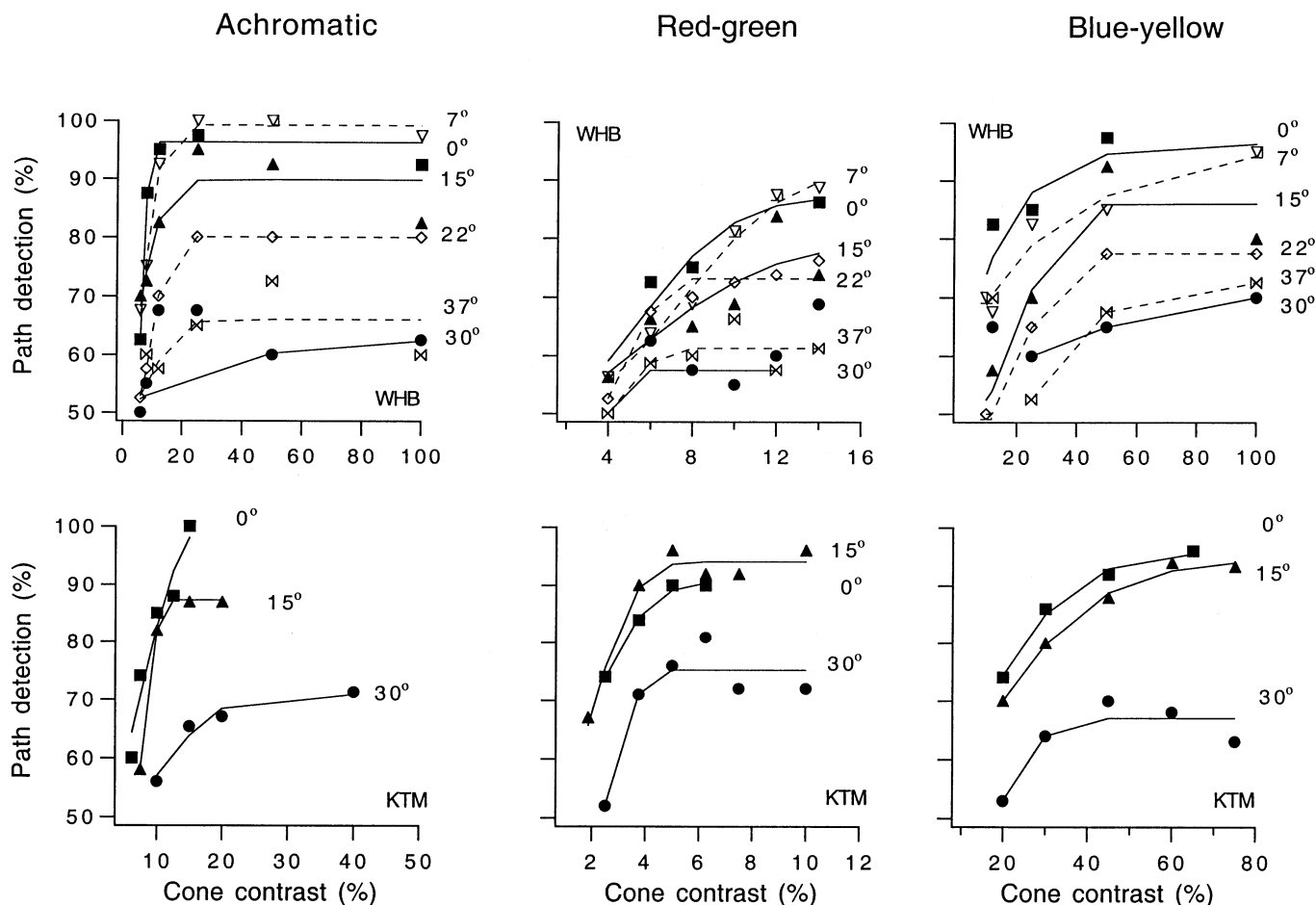


Fig. 3. Path detection (%) is plotted as a function of cone contrast in the three cardinal directions as marked. Each different function shows the results for a different path angle, ranging from 0 to 37° for WHB and 0 to 30° for KTM. Results for two subjects WHB (upper panels) and KTM (lower panels). The number of trials was 40 per data point for achromatic and blue–yellow stimuli and 80 for red–green stimuli for WHB, and for KTM 50 trials per data point. Solid and dashed lines show the fit of the modified Weibull function (see text).

individual red–green, blue–yellow and achromatic Gabor elements². Since path detection requires the integration of information across many different locations in the visual field, we measured Gabor detection thresholds at three eccentricities (0, 2 and 4° nasally from the fovea). Comparing these thresholds with those for path detection confirmed that the individual Gabor elements were always suprathreshold at path detection threshold. Their contrast at path detection threshold falls in the range of one to five times their own individual threshold, depending on the field location. Thus a somewhat higher contrast is required for the extraction of the contour than for the detection of the individual elements. We conclude that path detection is not limited by an inability to see the individual elements and the contrast limitation occurs at higher stage.

² Detection thresholds for the Gabor elements were measured on the same screen as used for path detection. The contrast resolution limit was overcome by generating single Gabor stimuli using a VSG2/4 framestore with 15 bit contrast resolution, housed in a Pentium PC computer.

3.2. The roles of contrast and curvature

We next investigated the combined role of contrast and path curvature in limiting contour integration. Path detection was measured over a range of cone contrasts and path curvatures (α) (Fig. 3). Six different curvatures from 0 to 37° were used for WHB, and three for KTM. Performance as a function of contrast shows a rapid rise in path detection followed by a saturation. The level at which performance asymptotes depends on the path curvature such that the best achievable path detection declines as curvature increases. These effects were quantified by fitting the data of Fig. 3 with Weibull functions corrected to take the asymptotic level into account:

$$PC(x) = pc_{\max} - (pc_{\max} - 50) \times e^{-(x/a)^b} \quad (2a)$$

where PC is percent correct, pc_{\max} is the asymptotic performance level, a is threshold performance, b is the slope, and x is contrast. The asymptotic parameter pc_{\max} reflects the optimum performance of the fitted

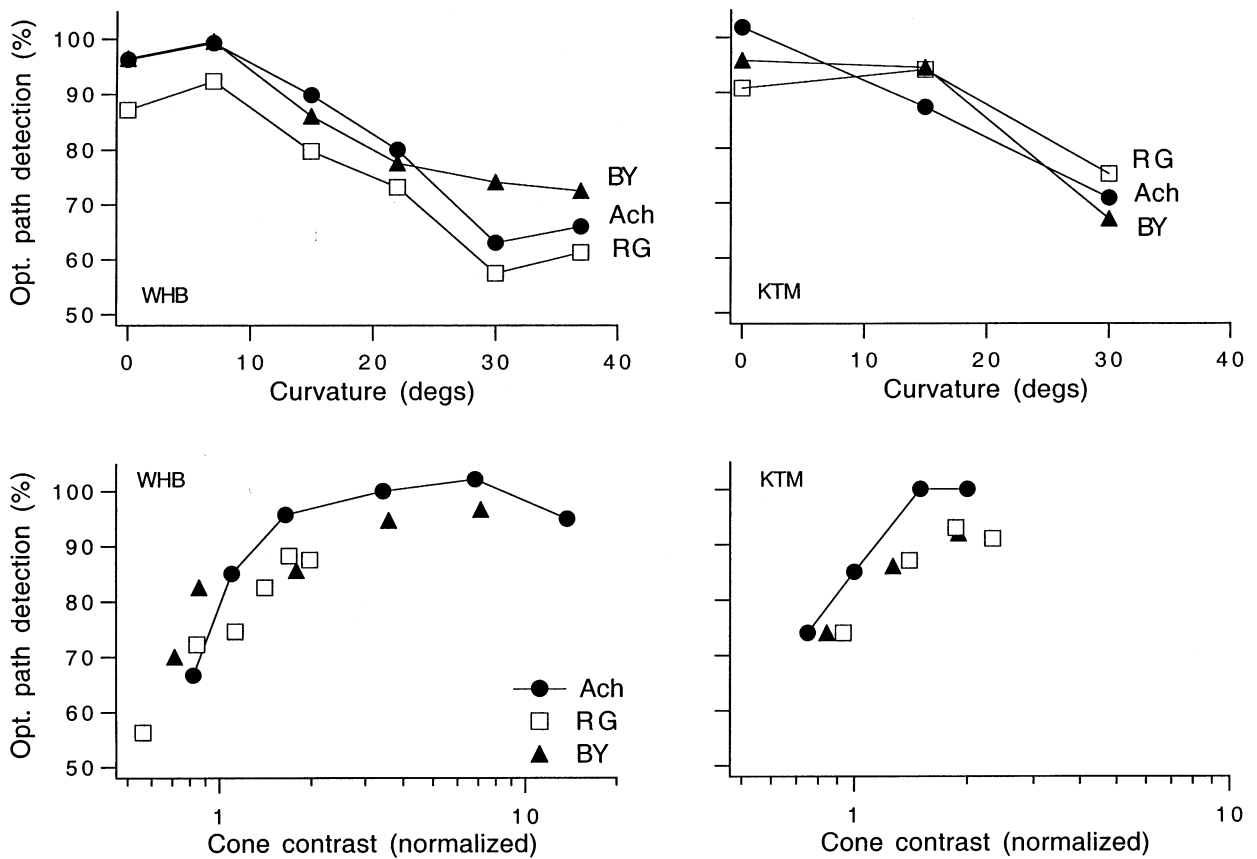


Fig. 4. All data points have been derived from the fitting of the modified Weibull function to the data of Fig. 3 (see text). Top panels: Fitted optimum path detection ($p_{c_{max}}$) as a function of path curvature for the three cardinal stimuli. Lower panels: Fitted optimum ($p_{c_{max}}$) path detection plotted as a function of normalized cone contrast for the three cardinal stimuli. Cone contrast is normalized to path detection threshold for a 0° path for each mechanism. WHB: left panels; KTM, right panels.

data set. Note that with this corrected function, threshold represents the relative position between chance (50%) and asymptotic values ($p_{c_{max}}$) and not a fixed detection value of 81.6% correct³. A corrected Weibull function is used because the data range is compressed by the influence of path curvature. Such functions have been used previously in analogous situations (Graham, 1989).

We have already shown in Fig. 2 that the three mechanisms display different path detection thresholds in terms of cone contrast; sensitivity in units of cone contrast is much better in the red–green and achromatic directions compared to the blue–yellow one. We argue, however, that comparing cone contrast thresholds across different color channels in order to conclude that one is better than another is not especially meaningful for this task. Instead we select a metric that allows the effects of contrast to be eliminated; in Fig. 4 (top panels) we plot the fitted asymptotic (optimal) performance ($p_{c_{max}}$) against path

curvature for the three mechanisms. This metric allows us to compare performance when the differences in contrast thresholds between the mechanisms have been compensated for: each mechanism is given the opportunity to perform as well as possible by raising its contrast as high as is necessary for performance to asymptote. Results show that for all three mechanisms, asymptotic performance levels decrease as curvature increases, in keeping with results reported previously for the achromatic and red–green mechanisms (Field et al., 1993; McIlhagga & Mullen, 1996). Curvature thus increases the difficulty of the task for all mechanisms, and this loss in performance cannot be compensated by an increase in stimulus contrast. For KTM, all three mechanisms have similar asymptotic (optimal) performance values. For WHB the performance of the red–green mechanism falls consistently below the other two; as discussed below this may be because the screen contrast for his red–green mechanism could not be raised high enough to obtain the full asymptotic value. Overall, from these results we make the preliminary conclusion that at suprathreshold contrasts the three mechanisms perform similarly on contour integration.

³ Threshold is 0.632 of the asymptotic level relative to chance level. For a $p_{c_{max}}$ of 100% this threshold corresponds to 81.6% correct.

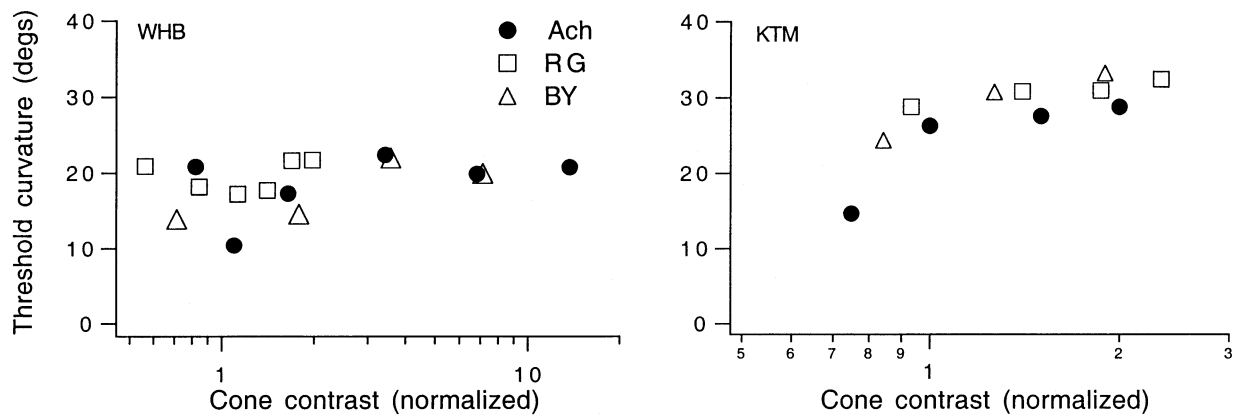


Fig. 5. All data points have been derived from the fitting of the modified Weibull function to the data of Fig. 3. Threshold path curvature ($^{\circ}$) is plotted as a function of normalized cone contrast for the three cardinal stimuli. Cone contrast is normalized to path detection threshold for a 0° path for each mechanism.

Next, using the data of Fig. 3, we fitted performance versus curvature to obtain a curvature threshold and asymptotic performance (pc_{\max}) at each fixed contrast. Since performance is inversely dependent on curvature, the Weibull function was adjusted to take this into account, and the threshold set so that it represents the same relative position between asymptotic and chance values as before⁴. The lower panels of Fig. 4 show the dependence of asymptotic (optimal) performance on cone contrast. Note that this metric allows us to compare between mechanisms when the effects of path curvature have been eliminated: each mechanism is given the opportunity to perform as well as possible by straightening the path as much as is necessary to reach asymptotic performance. At suprathreshold contrasts of approximately two to three times path detection threshold, asymptotic performance has reached a constant level. Overall, the achromatic mechanism has the best suprathreshold detection values (exceeding 95%), whereas the two chromatic mechanisms produces lower optimum detection values, spanning 88–96%. For WHB, the optimum performance for the red–green mechanism may be affected by the fact that the screen contrast could not be raised above two times path detection threshold: his red–green asymptotic performance is lower than for the other two mechanisms in both upper and lower panels but might improve if higher cone contrasts could be obtained⁵.

⁴ The Weibull used to fit declining performance with curvature is:

$$PC(x) = 50 + (pc_{\max} - 50) \times e^{- (x/a)^b} \quad (2b)$$

Parameters are as in Eq. (2a), except that x is now path curvature. The threshold (a) of this function is 0.368 of the asymptotic level relative to chance, and so was corrected back to 0.632 with the following formula:

$$\text{Curvature threshold} = a[-\ln(1 - e^{-1})]^{1/b}$$

⁵ Higher cone contrasts are unobtainable since the maximum cone contrast for the red–green mechanism is limited by the spectral emissions of the phosphors of the display monitor and the cone spectral absorbencies.

From the same fits (performance vs curvature for a fixed contrast) we obtained a threshold curvature (Fig. 5). This threshold indicates the curvyness of the path required for criterion detection and is plotted as a function of cone contrast. Within each subject, threshold curvatures are similar for the three postreceptoral mechanisms. Mean threshold curvatures calculated from the three highest contrasts of Fig. 5 are: for WHB, $21 \pm 1.3^{\circ}$ (achromatic), $19 \pm 3.8^{\circ}$ (blue–yellow), and $20 \pm 2.3^{\circ}$ (red–green); and for KTM, $28 \pm 1.2^{\circ}$ (achromatic), $30 \pm 4.6^{\circ}$ (blue–yellow) and $31 \pm 0.9^{\circ}$ (red–green). Thus within each subject the three mechanisms have no significant differences in their curvature thresholds, suggesting that the same inherent limitations within the linking process apply to each mechanism.

The data of Fig. 5 also show that, once path contrast is suprathreshold, increasing contrast does not improve the curvature threshold. In a further analysis (results not shown) we have also shown that cone contrast thresholds for path detection do not depend on its curvature.

In summary, we draw two conclusions; firstly that there is no interaction between the effects of contrast and curvature in limiting contour integration. This is because increasing contrast cannot compensate for losses in performance due to path curvature, and reducing curvature does not affect losses due to insufficient contrast. Secondly, we find that although the overall performance level of the chromatic mechanisms is slightly reduced compared to the luminance mechanism, there is no basis for considering the chromatic mechanisms as impaired on contour integration.

3.3. Role of foveal and parafoveal vision in contour integration

In this section, we examine the dependence of path integration on visual field location. We constrained the

path to pass through different regions of the $14 \times 14^\circ$ stimulus field. ‘Foveal’ path stimuli are defined as having at least one of the path elements within a central stimulus region 3° in diameter. Eccentric path stimuli were constrained to pass through different peripheral zones. These zones were defined as annular regions 1° wide and 3, 6 or 8° in diameter. At least one path element was constrained to pass through the annular region, and none could pass through its central ‘exclusion zone’. Relatively straight paths (0°) were used.

Results (Fig. 6) show that achromatic path detection is relatively flat across the whole stimulus field. Blue–yellow path detection is also relatively flat out to a radius of 3° from the fovea, but by 4° both subjects show a small rise in path detection threshold. The red–green path performance, however, shows a much stronger and consistent rise in threshold across the visual field, with a maximum threshold increase occurring at the most peripheral path location measured of

2.7 times foveal threshold for KTM and 1.8 times foveal threshold for WHB. This effect is consistent with the different patterns of contrast sensitivity loss for the three mechanisms in which the red–green mechanism displays a much steeper loss in contrast sensitivity across the visual field compared to the other two (Mullen, 1991; Mullen & Kingdom, 1996). Although the path elements are above their individual detection thresholds, the relatively strong decline in suprathreshold contrast may serve to weaken the linking process in the red–green mechanism.

3.4. Role of orientation discrimination in contour integration

Since contour integration depends on the linking of orientation across space, orientation is a likely factor which may limit performance on the task. We assessed the performance of the three mechanisms on an orientation discrimination task for a single Gabor element. Since we are interested in the interaction of orientation and path detection, the contrast of the Gabor was set to path detection threshold for each field location tested, using the data from Fig. 6.

Orientation discrimination was measured using a temporal 2AFC method of constant stimuli. The observer was shown two Gabor elements one after the other. The first Gabor element was randomly oriented between 85 and 95° (90° is vertical) and the second was $\pm x^\circ$ from the first. Each stimulus was displayed for 500 ms with a 1 s inter-stimulus interval. The observer decided if the second element was rotated left or right with respect to the first. Orientation discrimination threshold was determined from a Weibull fit of the data.

For both subjects, the results (Fig. 7) show that the red–green and achromatic mechanisms have similar orientation discrimination thresholds at path detection threshold, and these remain relatively flat out to 4° of eccentricity. Overall, the orientation discrimination thresholds for the blue–yellow mechanism are significantly higher than for the other two, indicating that the blue–yellow mechanism is poorer at encoding orientation. In addition, we measured the foveal orientation discrimination on two more subjects. The averaged data for four subjects are shown in the histogram inset and confirm that orientation discrimination at path detection threshold is significantly worse for the blue–yellow mechanism.

It is interesting to note how these orientation discrimination thresholds compare with path curvature thresholds (Fig. 4). Path curvature thresholds are approximately 20° for WHB and 30° for KTM. Yet, Fig. 7 shows that these orientation differences between individual elements are well above the Gabor orientation discrimination thresholds and so can easily be distin-

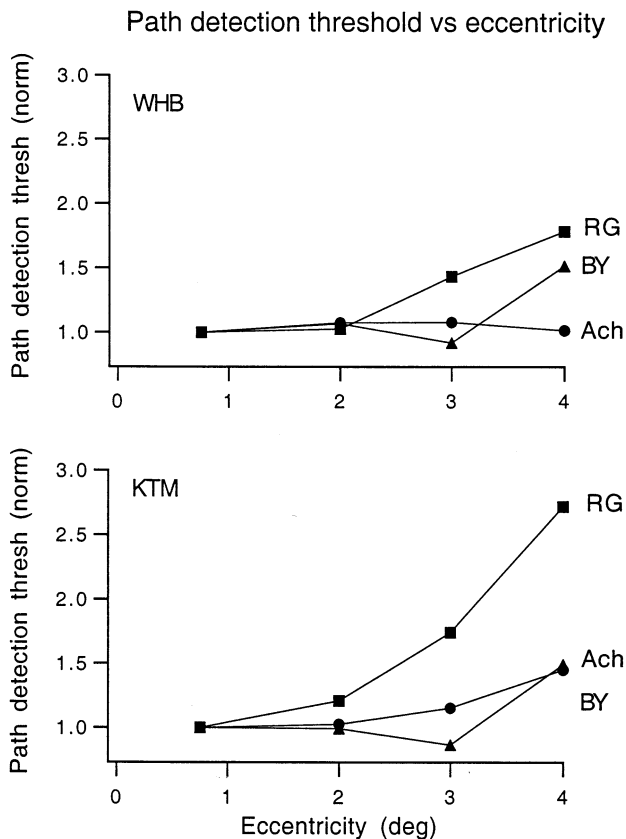


Fig. 6. Path detection thresholds, normalized to the foveal value for each subject and condition, are plotted as a function of the location of the path within the stimulus field (see text). Results for the three cardinal stimuli and two subjects. Thresholds were derived from the fit of a Weibull function based on five to six contrast levels and 120 trials each for WHB, and four to five contrast levels and 40 trials each for KTM.

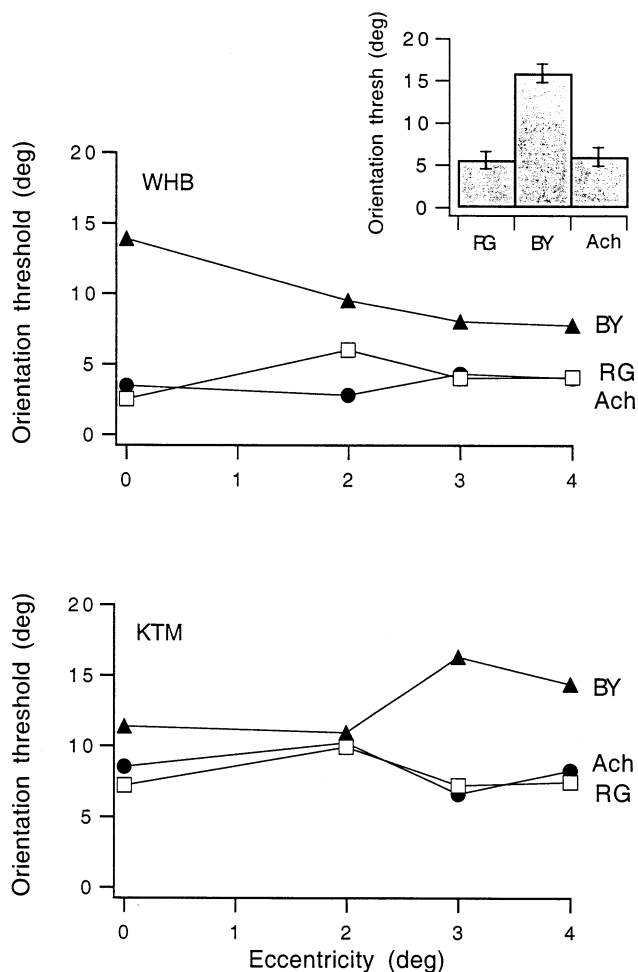


Fig. 7. Main panels: Orientation discrimination threshold for a single Gabor stimulus presented at different locations in the visual field. The contrast of the Gabor stimulus was set to the path detection threshold (0° path). For WHB reliable data for BY at the fovea could not be obtained during this experiment because of stimulus fading. Instead a measurement obtained during a previous experiment under the same conditions has been used. For KTM, the contrast of the blue–yellow stimulus was raised to 1.25 times path detection threshold to prevent fading of the stimulus. Results for the three cardinal stimuli and two subjects. Viewing was monocular (nasal field) for KTM and binocular for WHB. Thresholds were obtained using a method of constant stimuli with six to eight fixed Gabor orientations with ten trials per angle for WHB, and four fixed orientations with 30–50 trials per angle for KTM. For WHB orientation discrimination thresholds averaged across eccentricity are: 9.8 ± 2.8 (blue–yellow), 4 ± 1.4 (red–green), 3.7 ± 0.7 (achromatic) and for KTM the equivalent values are 13.3 ± 2.5 , 8 ± 1.3 , $8 \pm 1.5^\circ$. Inset: Orientation discrimination thresholds for a single Gabor stimulus foveally and monocularly fixated and presented at path detection threshold for all subjects. Data are the average for four observers (KTM, WHB, plus two additional experienced psychophysical observers with normal color vision). Error bars show ± 1 S.D.

guished. Furthermore, the blue–yellow mechanism shows no deficit in curvature threshold or optimum path detection in comparison to the other two mechanisms (Figs. 4 and 5), yet this mechanism is clearly poorer than the other two at discriminating the orienta-

tion of the individual Gabor elements. This results suggests that performance on the contour integration task is not restricted by a failure to resolve the orientation of the individual elements but is limited more centrally by the process of linking the elements into a contour.

3.5. Roles of orientation noise in limiting contour integration

We next compare the role of orientation noise in limiting path detection in the three postreceptoral mechanisms. Clearly, path detection will be disrupted if the orientation of the elements along the path ‘backbone’ is varied, since the common orientation of the path elements is being degraded. Stimuli were set to suprathreshold contrast levels of two times threshold for WHB and 2.2 times threshold for KTM. This is the highest contrast value that can be displayed on the monitor for the red–green mechanism and the contrasts of the other mechanisms were matched to this in multiples of threshold. At this contrast level, performance has asymptoted and contrast is not limiting performance. Orientation noise was created by adding a Gaussian distributed variance (σ^2) to the orientation of the path elements along the backbone (β in Fig. 1). A fixed orientation jitter of $\pm 10^\circ$ in path curvature ($\Delta\alpha$) is already present, and the orientation variance added to β combines with this pedestal value.

Results for the path curvatures (0, 15, and 25 or 30°) are shown in Fig. 8 for two subjects. For WHB this represents only a subset of the data as results for two additional path curvatures (7 and 22°) were collected. Each data point represents 100–200 trials. Results show that path detection decreases as orientation noise increases, as expected. The amount and form of disruption of the task by the applied orientation noise can theoretically be predicted from an ideal observer analysis which would yield values for the internal orientation noise and efficiency for the task. An ideal observer, however, has not yet been worked out for contour integration.

In lieu of this analysis, we fitted the data with a formula that adequately describes how performance depends on the signal/noise ratio of the stimulus orientation. Below we show its derivation:

$$d'_{\text{real}} \propto \frac{\sqrt{kS}}{\sqrt{\sigma_i^2 + \sigma_o^2 + \sigma_e^2}} \quad (3)$$

where σ_e^2 represents the added external noise, σ_i^2 represents the internal orientation noise of contour integration, σ_o^2 represents all other fixed sources of noise in the stimulus (e.g. backbone length jitter, backbone orientation jitter, noise from the background elements). We are assuming that all noise sources are independent and have additive effects on total variance. k is a sampling

efficiency parameter. S is the signal defined by the path curvature (α). The signal strength S is fixed across trials in a given condition and is independent of α . (The ideal observer will perform equally well for all path curvatures as the curvature of the path is known, and all curvatures are equally good signals.)

To convert from d' to percent correct we use the normal integral of $d'/2$:

$$PC = \Phi\left(\frac{d'}{2}\right) \quad (4)$$

and the function used to fit the data is:

$$PC = \Phi\left(\frac{C\sqrt{k}}{2\sqrt{\sigma_i^2 + \sigma_o^2 + \sigma_e^2}}\right) \quad (5)$$

where C is the product of an unknown proportionality constant and the fixed signal strength S , required because the magnitude and units of S are unknown.

The least squares weighted fits of this function to the data are shown by the solid lines (Fig. 8). The associated Q values for each fit are given in the figure legend.

Q is a χ^2 distribution function which gives the probability that the minimum χ^2 is as large as it is purely by chance. For small Q values the deviation from the model is unlikely to be due to chance and the model may be incorrect. For larger Q values, the deviation from the model is more likely to arise by chance suggesting the model is an adequate description of the data. A $Q0.1$ suggests an acceptable model fit (Press, Teukolsky, Vetterling & Flannery, 1992). For the data shown in Fig. 8, most (10/18) of the Q values indicate a statistically acceptable fit. For all the data, including the two curvatures for WHB not shown, 15/24 of the Q values are acceptable.

The primary aim of the fit is to compare the effects of added orientation noise between the three mechanisms. From the above formula we compare two sets of parameters for each path curvature and mechanism (Fig. 9). In the upper panels we plot the combined internal variance and fixed stimulus variance ($\sigma_o^2 + \sigma_i^2$) as a function of path curvature. Since the value of σ_o^2 is unknown we cannot estimate σ_i^2 separately. In the

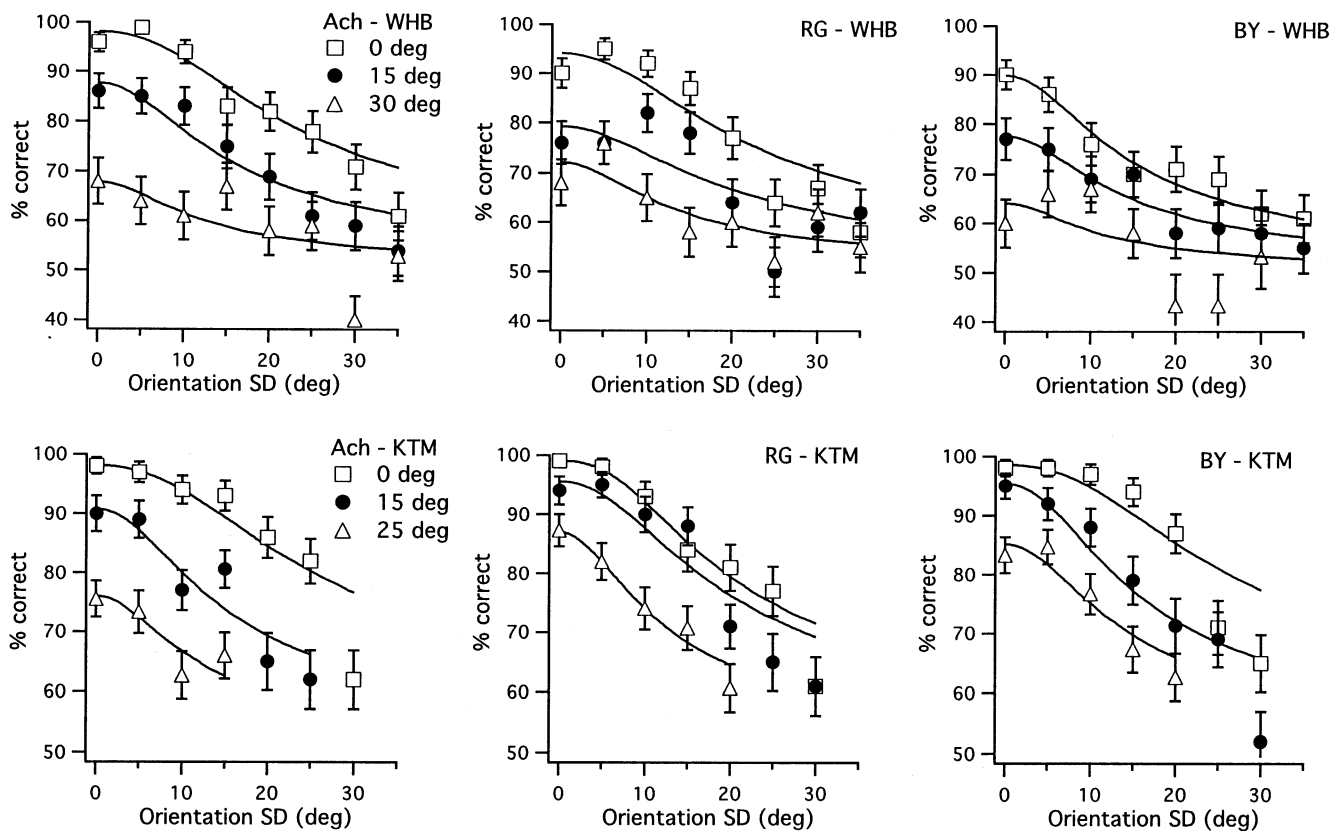


Fig. 8. Path detection as a function of the standard deviation of external orientation noise added to the stimulus (σ_e). Data are shown for the three postreceptoral mechanisms (Ach, RG & BY) and three path curvatures as marked. Orientation noise is the orientation variance (σ_o^2) added to the alignment of each element along the 'backbone' of the path (angle β in Fig. 1). Solid lines give the fits of the noise model. Two further functions were obtained for WHB, for path curvatures of 7 and 22°. The contrast of the stimulus was suprathreshold: set to 2.2 times path detection threshold for KTM and two times detection threshold for WHB for a path curvature of 0°. Data points are based on 100–200 trials each. Error bars give the binomial standard deviation. Q values for each fit were calculated and are as follows: WHB: Ach 0.06 (0°), 0.43 (15°), 0.05 (30°); RG 0.02 (0°), 0.01 (15°), 0.42 (30°); BY 0.94 (0°), 0.91 (15°), 0.05 (30°); and KTM: Ach 0.04 (0°), 0.13 (15°), 0.39 (30°); RG 0.37 (0°), 0.03 (15°), 0.72 (30°); BY 0.01 (0°), 0.10 (15°), 0.43 (30°).

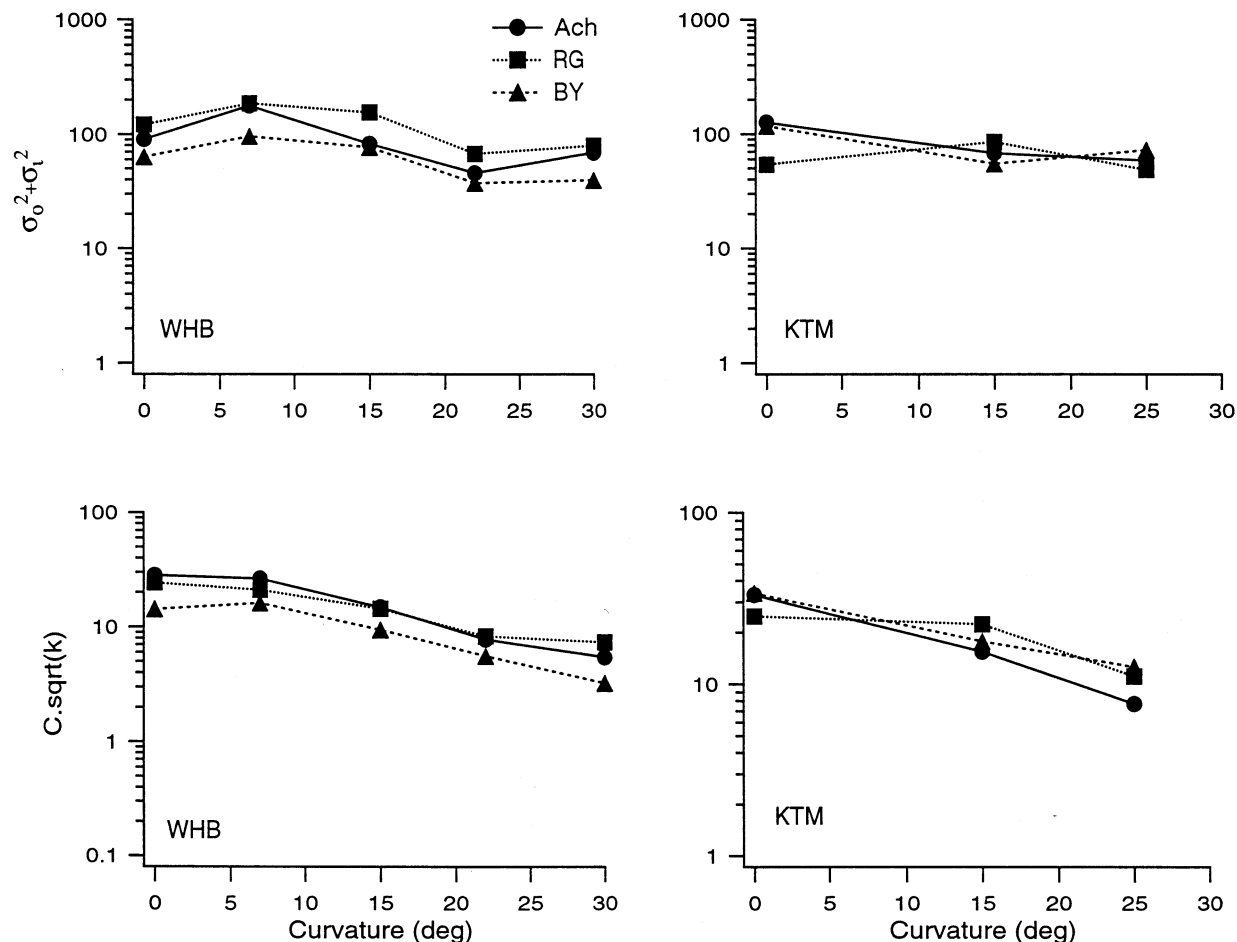


Fig. 9. Parameters for the fit of the data of Fig. 8 with the noise model of Eq. (5). In the top panels fitted values for combined internal orientation noise and fixed stimulus noise are plotted ($\sigma_0^2 + \sigma_i^2$) as a function of path curvature. In the lower panels the parameters ($C\sqrt{k}$) are plotted as a function of path curvature for the three mechanisms. See text for further details.

lower panels we plot the fitted value of $C\sqrt{k}$ as a function of curvature. Since C is unknown k cannot be plotted separately.

Results show that $(\sigma_0^2 + \sigma_i^2)$ remains relatively constant across the RG, BY and Ach mechanisms and across different curvatures. Since the fixed stimulus noise (σ_0^2) is invariant across the different chromatic stimuli or path curvatures, our data imply that the internal noise remains constant across the different mechanisms and curvatures. The fitted values of $C\sqrt{k}$ are also very similar between mechanisms with the exception that the value for the BY mechanism is a little lower for WHB, although this is not found for KTM. As path curvature increases $C\sqrt{k}$ shows a shallow decline. Since our stimuli are matched in their suprathreshold contrast values, we assume that signal strength is constant across mechanisms and that C is constant for our conditions. Under this assumption our results imply that efficiencies are similar for the three mechanisms but show a shallow decline with curvature. The decline in k with curvature is not surprising since the visual system is clearly less able to extract the

information from the stimulus for the more curvy paths.

3.6. Linking across different color mechanisms

McIlhagga and Mullen (1996) reported that contour integration between isoluminant red–green and achromatic Gabor elements was very poor. They used path stimuli with the two element types in alternating sequence and a random mixture of isoluminant red–green chromatic and luminance elements in the background. We address two further questions arising from these results. Firstly, we ask whether contour integration between elements differing only in color shows a similar impairment to that found for integration between color and luminance elements. Secondly, we consider whether the cardinal axes have any special status in contour integration: is linking more impaired for elements alternating between the two chromatic cardinal axes than for elements alternating between two intercardinal chromatic axes?

The left panel of Fig. 10 gives the cardinal color space used. Stimuli were all isoluminant. The abscissa is the red–green isoluminant axis, as determined for each subject, and the ordinate is the *S*-cone axis. The aspect ratio of the two axes has been scaled according to the subject's respective path detection thresholds for stimuli along each axis (square symbols). The two intercardinal axes (IC_1 and IC_2) lie at 45° to the two cardinal axes.

Stimuli were composed of a mixture of two types of Gabor element drawn from these four axes: for the path, the elements are in an alternating sequence, and for the background, the elements are randomly assigned as one type or the other. Contrasts were all set to the respective path detection thresholds. Note that the positive and negative parts of each axis were treated separately so that both phases of each chromatic stimulus (0 and 180°) were included. Results are shown for two subjects in the middle and right panels of Fig. 10. Path detection is plotted as a function of the separation between the elements in the cardinal color space. Thus if all elements are from a single axis, they are plotted at the 0° point, elements combined into a path from two adjacent axis in the color space are plotted at the 45° . Paths composed of elements that are 90° apart in the color space may be made up of alternating cardinal elements (red–green and blue–yellow) or alternating intercardinal el-

ements as shown by the different symbols (see legend for details).

Optimum performance occurs when stimulus elements are all from the same color direction. Alternating the phases (0 and 180°) of these path elements, however, causes a considerable reduction in performance, consistent with a previous report (McIlhagga & Mullen, 1996). When elements are from different color directions, the path also becomes more difficult to detect. We analyzed these effects using one and two way ANOVA tests with a Tukey/Kramer post-hoc analysis. For both subjects a significant loss in performance ($P < 0.05$) occurs when the path elements alternate between two directions in color space, compared to when elements are all from the same color direction. It makes no significant difference whether the elements are alternated between adjacent ($\Delta 45^\circ$) or orthogonal color axes. To compare intercardinal and cardinal orthogonal pairings, data was pooled across subject because of the low number of data points (triangles versus circles). We found no significant difference in performance between the cardinal and intercardinal pairings. Overall, our results show that any difference in the color appearance of alternating path elements reduces path detection, and there is no evidence for a privileged role for the cardinal axes.

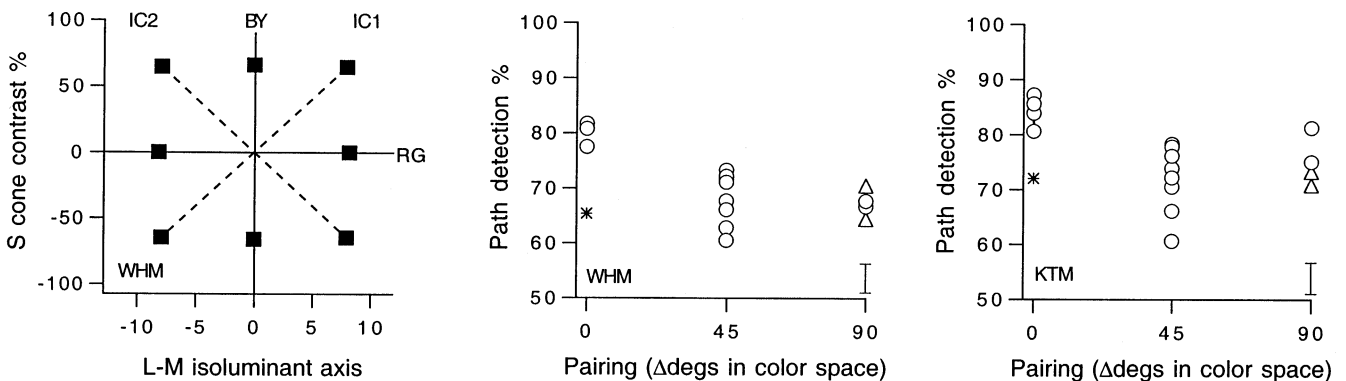


Fig. 10. Left panel shows the color space used to specify the colors of the alternating path elements. The ordinate is *S* cone contrast (%) and the abscissa is cone contrast (%) on the red–green isoluminant axis (determined for each subject). Data points show path detection threshold measured within this isoluminant plane in two cardinal directions (the red–green axis (RG), and blue–yellow (BY)) and two intercardinal directions (IC_1 and IC_2). Data were obtained for subjects KTM and WHM, results for WHM shown. Middle and right panels. Path detection (% correct) is plotted for different combinations of color contrasts of the Gabor elements, presented in alternating sequence. The pairs of color contrast used are specified by their separation in the color space used. Note that only two colors are used in the stimulus, drawn from the four color axes shown in the left panel. A pairing of 0° indicates that the Gabor elements of the stimulus were all drawn from the same direction in color space (four data points indicate the four possible types of path; BY, RG, IC_1 , IC_2). Circles indicate all the elements of the path were of the same phase. The star shows the data for phase alternating combinations, averaged across the four color axes. A pairing of 45° indicates path elements were from adjacent axes in color space. The eight plotted data points represent all four combinations of adjacent axes in two possible phases. Pairing of 90° means that path elements alternated between Gabor elements drawn from orthogonal axes in color space. These were either cardinal pairs (triangles: RG with BY) or intercardinal pairs (circles: IC_1 with IC_2). Both phase combinations are shown giving four data points in total. The contrast of the stimulus is set to path detection threshold. A path curvature of 0° was used for KTM, and 20° for WHM. Data represent the mean of three measurements, each based on 60 trials. The average S.D. of these means in percentage points is 5.3 for WHM and 5.7 for KTM, as shown each figure. Data were analyzed with an ANOVA test and post-hoc Tukey/Kramer analysis (see text).

4. Discussion

4.1. Evidence for a common integration process

Our results reveal more similarities than differences between the performances of the three postreceptoral mechanisms on the contour integration task. All three mechanisms are able to support contour integration. Although the optimum performances of the chromatic mechanisms fall slightly below that of the luminance mechanism (Fig. 4), there is no evidence that the chromatic channels can be considered deficient in contour integration. It is interesting that the performance of the blue–yellow mechanism on contour integration is not impaired in comparison to the other two mechanisms despite the fact that this mechanism is supported by a much sparser neural population. For example, the *S* cones are only around 7% of the total population (Curcio et al., 1991), and the postreceptoral neurons believed to be specialized for the *S* cone projections are relatively sparse, both subcortically (Dacey & Lee, 1994), and in the primary visual cortex (V1) (Ts'o & Gilbert, 1988). These differences in subcortical and early cortical sampling, however, do not appear to introduce any differential deficit in performance on the contour integration task, implying a more central limit on the integration process.

Another interesting similarity is that the achromatic, red–green and blue–yellow mechanisms require similar curvatures to reach path detection threshold: threshold curvature for each postreceptoral mechanism is around 20° for WHB and 30° for KTM, independent of contrast. This suggests that there are similar limitations to the linking process for all three mechanisms. A parsimonious explanation is that contour integration uses a common process drawing on the outputs of all three mechanisms.

In an attempt to understand the role of orientation in limiting path detection, we measured orientation discrimination thresholds for single Gabor stimuli at contrasts close to path detection threshold. We found that orientation discrimination for the blue–yellow mechanism is considerably poorer in comparison to the other two, even though the stimulus contrasts are equated for path detection threshold. On the other hand, there are no differences in path curvature thresholds between the three mechanisms. This implies that the visual system's accuracy at determining the orientation of individual Gabor elements is not limiting contour detection. Furthermore, we note that for all the mechanisms and visual field locations, the orientation discrimination thresholds of single Gabors are good (3–16°), demonstrating that the orientation of individual path elements can be specified regardless of whether this information can be used to link a contour.

We have also found that the three postreceptoral mechanisms are similarly affected by the addition of orientation noise, strengthening the argument that a similar integration process is used by all three mechanisms. An complete ideal observer analysis of contour integration which would allow the determination of absolute values for internal noise and sampling efficiency is not yet available. Instead we have fitted our functions with a formula that describes the dependence of performance on the addition of internal noise at different curvatures for the three mechanisms. Our results imply that the internal noise for the integration task is similar between the three mechanisms. This constant internal variability is specific to the linking task since it is not reflected in the orientation discrimination thresholds measured for the individual Gabor elements which show significant differences among mechanisms. Our results also imply that the relative sampling efficiencies are similar for the red–green, blue–yellow and achromatic mechanisms, revealing further similarities in contour integration between these three postreceptoral mechanisms. Finally, our results imply a loss of relative efficiency as path curvature increases, although further understanding and confirmation of this result will require development of a specific ideal observer model for path detection.

4.2. Impaired linking across postreceptoral mechanisms and phase

The arguments presented so far in favor of a common contour integration process require qualification in the light of our results showing that linking is sensitive to contrast type (color direction) and phase. The disruption of linking by elements alternating in their phase is contrary to the initial report by Field et al. (1993), which found no phase dependence, although a subsequent study reported that path detection was best with elements of constant contrast polarity (Field, Hayes & Hess, 1997). It is interesting that contour integration is disrupted by the phase alternation of our elements because it is an example of a loss of linking by alternation between elements that are similar in their appearance. In other words, the disruption of contour detection is not accompanied by a competing grouping effect, because elements of different phases do not visually segment from each other.

The second way of disrupting linking is by alternating the color direction of the path elements. Linking is disrupted by approximately the same amount regardless of whether the elements alternate between the two cardinal color directions, between the two intercardinal directions, or whether the alternating elements have smaller (45°) or larger (90°) color differences. These results demonstrate a lack of 'privilege' for the color cardinal axes in the disruption of the linking process

since any color change produces a similar loss in performance. This may imply that the inputs from the early postreceptoral mechanisms, which are independent at the level of detection threshold (Mullen & Sankeralli, 1999), are no longer independent at the stage of contour integration.

These results clearly demonstrate that the contour integration process is not ‘blind’ to the chromaticity of the elements. We can, however, rule out the possibility that there are three independent and parallel contour integration processes, one for each mechanism. As discussed by McIlhagga and Mullen (1996), an entirely parallel analysis would predict that an alternating ten element contour is seen as two separate contours of five elements each. Performance is near chance levels for such five element contours (McIlhagga & Mullen, 1996) and, taking into consideration probability summation occurring between two independently detected five element paths, predicted detection rates for a ten element alternating path fall in the range of 50–60%. Measured path detection rates for contours of alternating elements are consistently higher than this (see Fig. 10). Thus we conclude that the chromatic responses to the alternating elements are not treated independently, but are integrated in some fashion by a common contour process. The mixing of the mechanisms responses into the association field is, for some reason, disruptive to path integration.

4.3. Implications for the ‘association field’

In terms of Field et al. (1993), we would expect to find an ‘association field’ which distinguishes between different chromatic and luminance inputs, but requires inputs of all one type to fully function as an efficient contour integrator. The process might be considered as follows. Each individual element is described by its location, orientation, color contrast, and phase. The contour integrator computes a measure of association between all pairs of elements. The association is increased by common orientation and common color. This computation combines contrast information from all mechanisms at the same location. A path finding process searches through the associations to find those that are relatively high and links them together. If sufficient linking occurs, a path is seen.

4.4. Relationship to physiology

According to a recent physiological ‘binding’ model, path detection would be supported by cortical horizontal connections mediating context-dependent facilitatory and inhibitory interactions among oriented cells (Yen & Finkel, 1998). Strongly facilitated cells would mediate contour salience, possibly by temporal synchronization. Within this context, our results have two

possible explanations. Temporal synchronization might be relatively poor between the outputs of different postreceptoral mechanisms, and this might arise because they have different impulse response functions, with the achromatic mechanism having the shortest and the blue–yellow the longest (Metha & Mullen, 1996, 1997; Yoshizawa & Uchikawa, 1997). An alternative possibility arises from the proposal that long range horizontal cortical connections provide the means of modulating cell responses based on the structure of the surrounding scene (Gilbert, Das, Ito, Kapanda & Westheimer, 1996) and that these facilitate contour salience. There is evidence that horizontal cortical connections are selective for cells of similar orientation tuning (Toyama, Kimura & Tanaka, 1981a,b; Hata, Tsumoto, Sato, Hagihara & Tamura, 1993). Clearly, such a specificity might be extended to include the chromatic tuning of neurons, and this would provide a simple structural basis for the perceptual binding of similar elements into contours.

5. Conclusions

The blue–yellow and red–green cone opponent mechanisms support contour integration with very little impairment in comparison to the luminance mechanism, favoring an ‘intrinsic images’ view of color vision over the ‘coloring book model’ described in Section 1. We have argued for the existence of a common contour extraction process rather than the existence of a separate process for each postreceptoral mechanism. However, this process is not ‘color-blind’ since it is sensitive to the nature of its inputs. The question now arising is how chromatic and luminance inputs are used by a common process to generate an ‘intrinsic image’ for form perception.

Acknowledgements

This study was funded by a grant from the Medical Research Council of Canada to K.T. Mullen (MT-10819) and by a fellowship from the Fyssen Foundation to W.H.A. Beaudot. We gratefully acknowledge the contribution of Professor W.S. Geisler to the model described in Eqs. (3)–(5).

References

- Anstis, S., & Cavanagh, P. (1983). A minimum motion technique for judging equiluminance. In J. D. Mollon, & L. T. Sharpe, *Color vision: physiology and psychophysics*. London: Academic Press.
- Barrow, H. G., & Tennenbaum, J. M. (1978). Recovering intrinsic scene characteristics from images. In A. Hanson, & E. Riseman, *Computer vision systems*. New York: Academic Press.

- Bradley, A., Switkes, E., & De Valois, K. K. (1988). Orientation and spatial frequency selectivity of adaptation to color and luminance gratings. *Vision Research*, 28, 519–527.
- Bradley, A., Zang, L., & Thibos, L. N. (1992). Failures of isoluminance caused by ocular chromatic aberration. *Applied Optics*, 31, 2109–2148.
- Cole, G. R., & Hine, T. (1992). Computation of cone contrasts for color vision research. *Behavioural Research, Methods and Instrumentation*, 24, 22–27.
- Cole, G. R., Hine, T., & McIlhagga, W. H. (1993). Detection mechanisms in L-, M-, and S-cone contrast space. *Journal of the Optical Society of America A*, 10, 38–51.
- Curcio, C. A., Allen, K. A., Sloan, K. L., Lerea, C. L., Hurley, J. B., Klock, I. B., & Milam, A. H. (1991). Distribution and morphology of human cone photoreceptors stained with anti-blue opsin. *Journal of Comparative Neurology*, 312, 610–624.
- Dacey, D. M., & Lee, B. B. (1994). The 'blue-on' opponent pathway in primate retina originates from a distinct bistratified ganglion cell type. *Nature*, 367, 731–735.
- Elder, J., & Zucker, S. (1993). The effect of contour closure on the rapid discrimination of two-dimensional shapes. *Vision Research*, 33, 981–991.
- Field, D. J., Hayes, A., & Hess, R. F. (1993). Contour integration by the human visual system: Evidence for a local 'Association field'. *Vision Research*, 33, 173–193.
- Field, D., Hayes, A., & Hess, R. F. (1997). The role of phase and contrast polarity in contour integration. *Investigative Ophthalmology and Visual Science (Suppl.)*, 38, S999.
- Gilbert, C. D., Das, A., Ito, M., Kapanda, M., & Westheimer, G. (1996). Spatial integration and cortical dynamics. *Proceedings of the National Academy of Sciences USA*, 93, 615–622.
- Graham, N. V. S. (1989). *Visual pattern analyzers*. New York: Oxford University Press.
- Gregory, R. L. (1977). Vision with equiluminant colour contrast, 1. A projector technique and observations. *Perception*, 6, 113–119.
- Gregory, R. L., & Heard, P. F. (1989). Some phenomena and implications of isoluminance. In J. J. Kulikowski, C. M. Dickenson, & I. J. Murray, *Seeing contour and colour*. Oxford: Pergamon Press.
- Grossberg, S., & Mingolla, E. (1985). Neural dynamics of perceptual grouping: Textures, boundaries, and emergent segmentations. *Perception and Psychophysics*, 38, 141–171.
- Hata, Y., Tsumoto, T., Sato, H., Hagihara, K., & Tamura, H. (1993). Development of local horizontal interactions in cat visual cortex studies by cross-correlational analysis. *Journal of Neurophysiology*, 69, 42–56.
- Heitger, F., & von der Heydt, R. (1993). A computational model of neural contour processing: Figure-ground segregation and illusory contours. *Proceedings of the 4th International Conference on Computer Vision, Berlin*, IEEE Computer Society Press, Los Alamitos, CA.
- Hess, R. F., & Dakin, S. (1997). Absence of contour linking in peripheral vision. *Nature*, 390, 602–603.
- Kingdom, F. A. A., Moulden, B., & Collyer, S. (1992). A comparison between colour and luminance contrast in a spatial linking task. *Vision Research*, 32, 709–717.
- Kovacs, I., & Julesz, B. (1993). A closed curve is much more than an incomplete one: effect of closure in figure ground segmentation. *Proceedings of the National Academy of Sciences USA*, 90, 7495–7497.
- Krauskopf, J., & Farell, B. (1991). Vernier acuity: effects of chromatic content, blur and contrast. *Vision Research*, 31, 735–749.
- Livingstone, M. S., & Hubel, D. H. (1987). Psychophysical evidence for the perception of form, color, movement, and depth. *Journal of Neuroscience*, 7, 3416–3468.
- Livingstone, M. S., & Hubel, D. H. (1988). Segregation of form, color, movement and depth: anatomy, physiology and perception. *Science*, 240, 740–749.
- Losada, M. A., & Mullen, K. T. (1995). Color and luminance spatial tuning estimated by noise masking in the absence of off-frequency looking. *Journal of the Optical Society of America A*, 12, 250–260.
- Lu, C., & Fender, D. H. (1972). The interaction of colour and luminance in stereoscopic vision. *Investigative Ophthalmology*, 11, 482–490.
- Marr, D. (1982). *Vision*. San Francisco, CA: W.H. Freeman & Co.
- McIlhagga, W. H., Hine, T., Cole, G. R., & Snyder, A. W. (1990). Texture segregation with luminance and chromatic contrast. *Vision Research*, 30, 489–498.
- McIlhagga, W. H., & Mullen, K. T. (1996). Contour integration with color and luminance contrast. *Vision Research*, 36, 1265–1279.
- McIlhagga, W. H., & Mullen, K. T. (1997). The contribution of colour to contour detection. In C. M. Dickenson, I. Murray & D. Carden, *Colour vision research: Proceedings of the John Dalton Conference* (pp. 187–196). London: Taylor & Francis.
- Metha, A. B., & Mullen, K. T. (1996). Temporal mechanisms underlying flicker detection and identification for red-green and achromatic stimuli. *Journal of the Optical Society of America A*, 13, 1969–1980.
- Metha, A. B., & Mullen, K. T. (1997). Red-green and achromatic temporal filters: a ratio model predicts contrast dependent speed perception. *Journal of the Optical Society of America A*, 14, 984–996.
- Mullen, K. T. (1991). Colour vision as a postreceptoral specialization of the central visual field. *Vision Research*, 31, 119–130.
- Mullen, K. T., & Kingdom, F. A. (1990). Chromatic contrast and form perception. In: P. Gouras, *The perception of colour* (pp. 198–217). In: J. Cronly-Dillon, *Vision and visual dysfunction*, vol. 6. New York: Macmillan Press.
- Mullen, K. T., & Kingdom, F. A. (1996). Losses in peripheral color sensitivity predicted from 'hit & miss' postreceptoral cone connections. *Vision Research*, 36, 1995–2000.
- Mullen, K. T., & Sankeralli, M. J. (1999). Evidence for the stochastic independence of the blue-yellow, red-green and luminance detection mechanisms revealed by subthreshold summation. *Vision Research*, 39, 733–745.
- Parent, P., & Zucker, S. W. (1989). Trace inference, curvature consistency and curve detection. *IEEE Transactions on Pattern Analysis and Machine Intelligence*, 11, 823–839.
- Press, W. H., Teukolsky, S. A., Vetterling, W. T., & Flannery, B. P. (1992). *Numerical Recipes in C: the art of scientific computing* (2nd ed.). Cambridge: Cambridge University.
- Sankeralli, M. J., & Mullen, K. T. (1996). Estimation of the L-, M- and S-cone weights of the post-receptoral detection mechanisms. *Journal of the Optical Society of America A*, 13, 906–915.
- Simmons, D. R., & Kingdom, F. A. A. (1994). Contrast thresholds for stereoscopic depth identification with isoluminant and isochromatic stimuli. *Vision Research*, 34, 2971–2982.
- Switkes, E., Bradley, A., & De Valois, K. K. (1988). Contrast dependency and mechanisms of masking interactions among chromatic and luminance mechanisms. *Journal of the Optical Society of America A*, 5, 1149–1162.
- Toyama, K., Kimura, M., & Tanaka, K. (1981a). Cross-correlation analysis of interneuronal connectivity in cat visual cortex. *Journal of Neurophysiology*, 46, 191–201.
- Toyama, K., Kimura, M., & Tanaka, K. (1981b). Organization of cat visual cortex as investigated by cross-correlation technique. *Journal of Neurophysiology*, 46, 202–214.
- Ts'o, D. Y., & Gilbert, C. D. (1988). The organization of chromatic and spatial interactions in the primate striate cortex. *Journal of Neuroscience*, 8, 1712–1727.

- Webster, M. A., De Valois, K. K., & Switkes, E. (1990). Orientation and spatial frequency discrimination for luminance and chromatic gratings. *Journal of the Optical Society of America A*, 7, 1034–1049.
- Williams, D. R., Collier, R. J., & Thompson, B. J. (1983). Spatial resolution of the short wave mechanism. In J. D. Mollon, & L. T. Sharpe, *Color vision: physiology and psychophysics* (pp. 487–504). London: Academic Press.
- Yen, S. C., & Finkel, L. H. (1998). Extraction of perceptually salient contours by striate cortical networks. *Vision Research*, 38, 719–742.
- Yoshizawa, T., & Uchikawa, K. (1997). Temporal integration characteristics of chromatic response as determined by use of the isoluminant double-pulse method. *Journal of the Optical Society of America A*, 14, 2069–2080.